12-8-2015

Efficient high-order methods for solving fractional differential equations of order $\alpha \in (0, 1)$ using fast convolution and applications in wave propagation

Matthew F. Causley

Peter G. Petropoulus

Efficient high-order methods for solving fractional differential equations of order $\alpha \in (0, 1)$ using fast convolution and applications in wave propagation

Article · January 2016

CITATIONS
0

READS
118

2 authors:

Matthew F Causley
Kettering University
22 PUBLICATIONS **100** CITATIONS
SEE PROFILE

P. G. Petropoulos
New Jersey Institute of Technology
41 PUBLICATIONS **1,275** CITATIONS
SEE PROFILE

BIT manuscript No.
(will be inserted by the editor)

Efficient high-order methods for solving fractional differential equations of order $\alpha \in (0,1)$ using fast convolution and applications in wave propagation

Matthew F. Causley · , Peter G. Petropoulos

Received: date / Accepted: date

Abstract In this work we develop a means to rapidly and accurately compute the Caputo fractional derivative of a function, using fast convolution. The key element to this approach is the compression of the fractional kernel into a sum of M decaying exponentials, where M is minimal. Specifically, after N time steps we find $M = \mathcal{O}(\log N)$ leading to a scheme with $\mathcal{O}(N \log N)$ complexity. We illustrate our method by solving the fractional differential equation representing the Kelvin-Voigt model of viscoelasticity, and the partial differential equations that model the propagation of electromagnetic pulses in the Cole-Cole model of induced dielectric polarization.

1 Introduction

A popular model to fit experimentally measured frequency-dependent dielectric permittivity data is the Cole-Cole model [6] which exhibits frequency dependence of the form $(i\omega)^\alpha$, where $\alpha \in (0,1)$ and ω is the frequency (Section 5.2 herein, Eq. (5.3)). Once this frequency-dependent model is transformed to the time-domain, for the purpose of incorporating it in numerical solvers of the time-domain Maxwell equations, the constitutive relation between the electric field and the induced dielectric polarization becomes a fractional differential equation of order α (Section 5.2 herein, Eq. (5.7)) that involves the Caputo derivative [18]. Perhaps the most important use of the Cole-Cole model was made by Gabriel et. al [10], in which broadband measurements of the permittivity of various human tissues are fitted to multi-term Cole-Cole models, thus opening the way for the accurate simulation of ultra-wideband pulse propagation through the human body for purposes such as determining safety standards for exposure to the non-ionizing radiation from antennas [14,7].

In this paper we are focused on the numerical computation of Caputo fractional derivatives of order $0 < \alpha < 1$

$$D_t^\alpha u(t) = \int_0^t K_\alpha(\tau) u'(t-\tau) d\tau, \quad t \geq 0, \tag{1.1}$$

where the fractional kernel is defined as

$$K_\alpha(t) = \frac{t^{-\alpha}}{\Gamma(1-\alpha)}, \qquad 0 < \alpha < 1. \tag{1.2}$$

Our work also applies to the computation of fractional derivatives of higher order $m < \alpha < m+1$ (for integer $m > 0$), provided we replace u' with $u^{(m+1)}$ and α with $\beta = \alpha - m$ in the definition (1.1) noting

M. Causley
Kettering University
Tel.: (810) 762 9702
E-mail: mcausley@kettering.edu

P. Petropoulos
New Jersey Institute of Technology
Tel.: (973) 596-5626
E-mail: peterp@njit.edu

that the exponent β of the kernel remains in the interval $(0, 1)$. Therefore without loss of generality, we take $0 < \alpha < 1$, and consider fractional derivatives of arbitrary order.

In Sections 2 and 3 we focus on the fast and high-order accurate numerical evaluation of the fractional derivative (1.1). Section 4 provides numerical confirmation of the convergence rate of our method, and a comparison with the method in [16] which shows an order of magnitude reduction in the computational burden when using our approach. Finally, Section 5 applies our algorithm to the solution of fractional differential equations of the form

$$D_t^\alpha u = f(t, u), \qquad t > 0, \tag{1.3}$$

by solving the fractional differential equation representing the Kelvin-Voigt model of viscoelasticity (Section 5.1), and the partial differential equations that model the propagation of electromagnetic pulses in the Cole-Cole model of induced dielectric polarizaton (Section 5.2). For the latter application we also provide stability and phase error analyses of the discrete Maxwell system coupled to the herein discretized fractional differential equation representing the Cole-Cole model in the time-domain along with numerical results that verify the convergence rate of the overall algorithm.

2 Fast Convolution for the Caputo Fractional Derivative

Consider the computation of $D_t^\alpha u(t)$ for $t = t_1, t_2, \dots t_N$. The straightforward numerical computation of the Caputo fractional derivative (1.1) will require a discrete convolution of length n at each time level (or equivalently, the fractional differentiation matrix is dense [18]), leading to an $\mathcal{O}(N^2)$ complexity. This is in contrast to the $\mathcal{O}(N)$ scaling for computing an ordinary derivative at the same points (which can be represented by a sparse differentiation matrix). For this reason, we introduce fast convolution, which uses a low rank approximation of the fractional kernel (1.2) to compute the fractional derivative with $\mathcal{O}(N \log N)$ complexity. In order to accomplish this, we observe that the fractional kernel can be defined as an integral

$$K_\alpha(t) = \frac{1}{\Gamma(\alpha)\Gamma(1-\alpha)} \int_0^\infty y^{\alpha-1} e^{-yt} dy = \frac{\sin(\pi\alpha)}{\pi} \int_0^\infty y^{\alpha-1} e^{-yt} dy. \tag{2.1}$$

This integral can then be discretized to produce a sum of exponentials approximation, which can be made accurate to a desirable level over some fixed interval

$$K_\alpha(t) \approx K_\alpha^M(t) = \sum_{m=1}^{M} w_m e^{-y_m t}, \quad t \in [t_1, t_N], \tag{2.2}$$

where $t_1 > 0$. Then, the fractional derivative (1.1) can be decomposed [12] as

$$D_t^\alpha u(t) \approx \int_0^\delta K_\alpha(\tau) u'(t-\tau) d\tau + \int_\delta^t K_\alpha^M(\tau) u'(t-\tau) d\tau, \tag{2.3}$$

where we will eventually take $t = t_n$, and consider $\delta = \Delta t_n = t_n - t_{n-1}$.

Hereafter we will refer to the first integral in (2.3) as the "local contribution" and note that it is comprised of the most recent historical values of u. It may be tempting to neglect the local contribution of the integral, equivalently setting $\delta = 0$. But because $K_\alpha(t)$ is singular at $t = 0$, there will always be a region near $t \approx 0$ where (2.2) will no longer maintain accuracy, and so this local contribution cannot be accurately computed with the exponential sum. Thus, we can rewrite (2.3) using auxiliary variables

$$D_t^\alpha u(t) \approx \phi_0(t) + \sum_{m=1}^{M} w_m \phi_m(t) \tag{2.4}$$

where

$$\phi_0(t) = \int_0^\delta K_\alpha(\tau) u'(t-\tau) d\tau, \tag{2.5}$$

and

$$\phi_m(t) = \int_\delta^t e^{-y_m \tau} u'(t-\tau) d\tau, \qquad m = 1, 2, \dots M. \tag{2.6}$$

The sum in (2.4) will be hereafter referred to as the "history contribution." Upon differentiation of the ϕ_m, and rearranging, we find that they satisfy differential equations of the form

$$\phi_m'(t) + y_m \phi_m(t) = u'(t-\delta), \qquad m = 1, 2, \dots M. \tag{2.7}$$

Consequently, the integrals (2.6) need not be computed, as we can obtain $\phi_m(t_n)$ locally via any ODE integrator of choice, in $O(1)$ computations. This means that we can now obtain the fractional derivative of u up to time t_N in $O(MN)$ complexity. Thus, our goal is to make M as small as possible, and achieve a fractional derivative calculation that is almost as efficient as that of an ordinary derivative.

2.1 The local contribution

We first turn our attention to the local contribution of the fractional derivative. For $t = t_n$, we set $\delta = \Delta t_n = t_n - t_{n-1}$, and consider a Taylor series expansion of $u'(t-\tau)$ up to some power P, so that

$$\phi_0(t_n) = \int_0^{\Delta t_n} K_\alpha(\tau) u'(t_n - \tau) d\tau \approx \sum_{p=1}^{P} \frac{(-1)^p}{p!} a_p u^{(p)}(t_n), \tag{2.8}$$

where

$$a_p = \int_0^{\Delta t_n} K_\alpha(\tau) \tau^{p-1} d\tau = \frac{(\Delta t_n)^{p-\alpha}}{\Gamma(1-\alpha)(p-\alpha)}, \qquad p = 1, 2, \dots P. \tag{2.9}$$

To construct a numerical scheme, the derivatives are replaced with a finite approximation, which we accomplish with a collocation scheme. Our result is contained in the following lemma.

Lemma 2.1 *For $P \geq 1$, define the polynomial $\psi(\tau)$ of order P which interpolates $u(t_n - \tau) \in C^{P+1}$ at the points $\tau = \tau_p = t_n - t_{n-p}$, $p = 0, 1, \dots, P$, and is expressed in Lagrange form as*

$$\psi(\tau) = \sum_{p=0}^{P} u(t_{n-p}) \ell_p(\tau), \qquad \ell_p(\tau_q) = \delta_{pq}.$$

Then the approximation

$$\phi_0(t_n) = \sum_{p=0}^{P} c_p u(t_{n-p}), \qquad c_p = \int_0^{\Delta t_n} K_\alpha(\tau) \ell_p'(\tau) d\tau, \tag{2.10}$$

will be accurate to order $P + 1 - \alpha$. When $n < P$, the polynomial interpolates the points $t_0, \dots t_P$, and the same accuracy is achieved.

Proof Since $\psi(\tau)$ is an interpolating polynomial of degree P, we have [1]

$$u(t_n - \tau) - \psi(\tau) = \ell(\tau) \frac{u^{(P+1)}(\tau^*)}{(P+1)!}, \qquad \ell(\tau) = \prod_{p=0}^{P} (\tau - \tau_p),$$

where $\tau^* \in [\tau_0, \tau_P] = [0, (t_n - t_{n-P})]$. Upon differentiating, multiplying by $K_\alpha(\tau)$ and integrating, we find

$$\int_0^{\Delta t_n} K_\alpha(\tau) u'(t_n - \tau) d\tau = \sum_{p=0}^{P} c_p u(t_{n-p}) + C \frac{u^{P+1}(\tau^*)}{(P+1)!},$$

where the scaled local truncation error is

$$C = \int_0^{\Delta t_n} K_\alpha(\tau) \ell'(\tau) d\tau.$$

Substituting $\tau = z \Delta t_n$ and computing the integral, the local truncation error becomes

$$C = \frac{(\Delta t_n)^{P+1-\alpha}}{\Gamma(1-\alpha)} \int_0^1 z^{-\alpha} \hat{\ell}'(z) dz = C(\alpha, P) (\Delta t_n)^{P+1-\alpha},$$

where $\hat{\ell}(z)$ does not depend on Δt_n. Thus, we find the order is $P + 1 - \alpha$.

In this proof, we have taken u to be sufficiently smooth, and note that for monomials $u = t^\beta$ with non-integer β only a finite number of derivatives will be bounded. This will affect the rate of convergence, as is demonstrated with numerical examples in Section 4. Lemma 1 and its analog, Lemma 2, in Section 2.2 provide the means to obtain high-accuracy for the evaluation of the local and history contributions in the computation of the Caputo fractional derivative.

In order to utilize the scheme, we need then to construct Lagrange interpolating polynomials, and make use of (2.10) accordingly, as summarized in Algorithm 1. Note that if uniform time stepping is used, this construction is only used for the first P steps, and then the coefficients c_p are fixed.

Algorithm 1 Local quadrature rule

Given points t_{n-p} for $p = 0, 1, \dots P$,

1: Construct the $(P+1) \times (P+1)$ Vandermonde matrix V, where $V_{ij} = (t_n - t_{n+1-j})^{i-1}$.

2: Construct the vector $\mathbf{x}$, with $x_1 = 0$,

$$x_i = (i-1)a_{i-1}, \quad i = 2, \dots P+1,$$

and where a_i is defined by (2.9).

3: The coefficients $\mathbf{c} = (c_0, \dots, c_P)$ in the update scheme (2.10) are then computed by

$$\mathbf{c} = V^{-1}\mathbf{x}.$$

2.2 The history contribution

The equations (2.7) can be solved with any suitable (i.e., L-stable) ODE integrator. Since we will be solving the local contribution up to order P with a collocation scheme, we do the same here. Applying the integrating factor method, we first re-cast these equations as

$$\phi_m(t) = e^{-y\delta}\phi_m(t-\delta) + \int_0^\delta e^{-y_m\tau}u'(t-\delta-\tau)d\tau.$$

Setting $t = t_n$ and $\delta = \Delta t_n = t_n - t_{n-1}$, we again perform a Taylor series expansion up to order P, yielding the approximation

$$\phi_m(t_n) = e^{-y_m\Delta t_n}\phi_m(t_{n-1}) + \sum_{p=1}^{P} \frac{(-1)^p}{p!} a_{mp} u^{(p)}(t_{n-1}), \qquad m = 1, \dots M, \tag{2.11}$$

where the coefficients are

$$a_{mp} = \int_0^{\Delta t_n} e^{-y_m\tau}\tau^{p-1}d\tau = \frac{p!}{y_m^p}\left(1 - e^{-\nu_m}\sum_{k=0}^{p}\frac{\nu_m^k}{k!}\right), \quad \nu_m = y_m\Delta t_n, \qquad p = 1, \dots P. \tag{2.12}$$

We summarize our approach and state its convergence rate in the following lemma.

Lemma 2.2 *For $P \geq 1$, define the polynomial $\psi(\tau)$ of order P which interpolates $u(t_{n-1} - \tau) \in C^{P+1}$ at the points $\tau = \tau_p = t_{n-1} - t_{n-1-p}$, $p = 0, 1, \dots, P$, and is expressed in Lagrange form as*

$$\psi(\tau) = \sum_{p=0}^{P} u(t_{n-1-p})\ell_p(\tau), \qquad \ell_p(\tau_q) = \delta_{pq}.$$

Then the approximation

$$\phi_m(t_n) = e^{-y_m\Delta t_n}\phi_m(t_{n-1}) + \sum_{p=0}^{P} b_{mp}u(t_{n-1-p}), \qquad b_{mp} = \int_0^{\Delta t_n} e^{-y_m(\tau+\Delta t_n)}\ell_p'(\tau)d\tau, \tag{2.13}$$

will be accurate to order $P+1$. When $n < P$, the polynomial interpolates the points $t_0, \dots t_P$, and the same accuracy is achieved.

The proof of this lemma is analogous to that of Lemma 1, and is omitted. Likewise, the construction of the quadrature rule is very similar, as shown in Algorithm 2. As was the case with the local contribution, in the case of uniform time stepping, only the first P steps yield a different set of coefficients, and for $n > P$, they remain fixed.

Algorithm 2 History quadrature rule

Given points t_{n-1-p} for $p = 0, 1, \dots P$, and the exponentials y_m for $m = 1, \dots M$,

1: Construct the $(P+1) \times (P+1)$ Vandermonde matrix V, where $V_{ij} = (t_{n-1} - t_{n-j})^{i-1}$.

2: Construct the vectors $\mathbf{x}_m$, with $x_{m1} = 0$,

$$x_{mi} = (i-1)a_{m,i-2}, \quad i = 2, \dots P+1,$$

and where a_{mi} is defined by (2.12).

3: The coefficients $\mathbf{b}_m = (b_{m0}, \dots, b_{mP})$ in the update scheme (2.10) are then computed by

$$\mathbf{b}_m = V^{-1}\mathbf{x}_m.$$

3 Compressing the Fractional Kernel

We now construct a suitable sum of exponentials approximation (2.2), for which error estimates are readily available. This idea is not new, and has been studied in great detail [2,9,11,21], by employing various integration techniques. The most successful approaches appear to be that of [9] and [2]. We briefly review [9] in order to motivate our adopting the method in [2]. We also offer new insights into the overall construction of the sums in Section 3.7.

3.1 A quadrature rule with exponential accuracy

As a motivating platform, we first explore the method of [9], which arises from mapping the integral (2.1) from $y \in [0, \infty)$ to $z \in (-1, 1)$ and generalize it for our purpose. Let

$$y = \left(\frac{1+z}{1-z}\right)^p, \quad p > 0. \tag{3.1}$$

We note that the approach in [9] corresponds to $p = 2$, but other authors, e.g., [3], have used larger p. Applying this mapping, we find that

$$K_\alpha(t) = \frac{2p}{\pi}\sin(\pi\alpha)\int_{-1}^{1}\left(\frac{1+z}{1-z}\right)^{p\alpha}\frac{\exp\left(-t\left(\frac{1+z}{1-z}\right)^p\right)}{1-z^2}dz.$$

Notice that this integral can quite naturally be discretized using classical Gauss-Jacobi quadrature with weight function

$$\omega(z) = (1-z)^{p(1-\alpha)-1}(1+z)^{p\alpha-1}$$

yielding the approximation

$$K_\alpha^M = \frac{2p}{\pi}\sin(\pi\alpha)\sum_{m=1}^{M}\omega_m(1-z_m)^{-p}e^{-y_m t}, \tag{3.2}$$

where (ω_m, z_m) are the classical Gauss-Jacobi weights and nodes, and y_m is obtained from the mapping (3.1), evaluated at the nodes z_m.

A numerical study of the relative accuracy of this approximation as a function of t (as shown in Figure 3.1, for $M = 25$ points with $\alpha = 0.5$) revealed that for smaller values of p the approximation achieves exponential accuracy for $t \approx 1$, and falls off quickly otherwise. As p increases, the maximum error decreases, and the minimum error increases, essentially spreading the region in the neighborhood of $t = 1$ over the comparison time interval. This indicates that (3.2) has the potential to result in a uniform relative error over a prescribed computational interval. Motivated by this observation we study this phenomenon as p is increased further by first rescaling the variable $z \to z/2p$ and then taking the limit as $p \to \infty$, yielding

$$\begin{aligned} K_\alpha(t) &= \lim_{p\to\infty}\frac{1}{\pi}\sin(\pi\alpha)\int_{-2p}^{2p}\left(\frac{1+z/2p}{1-z/2p}\right)^{p\alpha}\frac{\exp\left(-t\left(\frac{1+z/2p}{1-z/2p}\right)^p\right)}{(1-z/2p)^2}dz \\ &= \frac{\sin(\pi\alpha)}{\pi}\int_{-\infty}^{\infty}\exp\left(\alpha z - te^z\right)dz. \end{aligned} \tag{3.3}$$

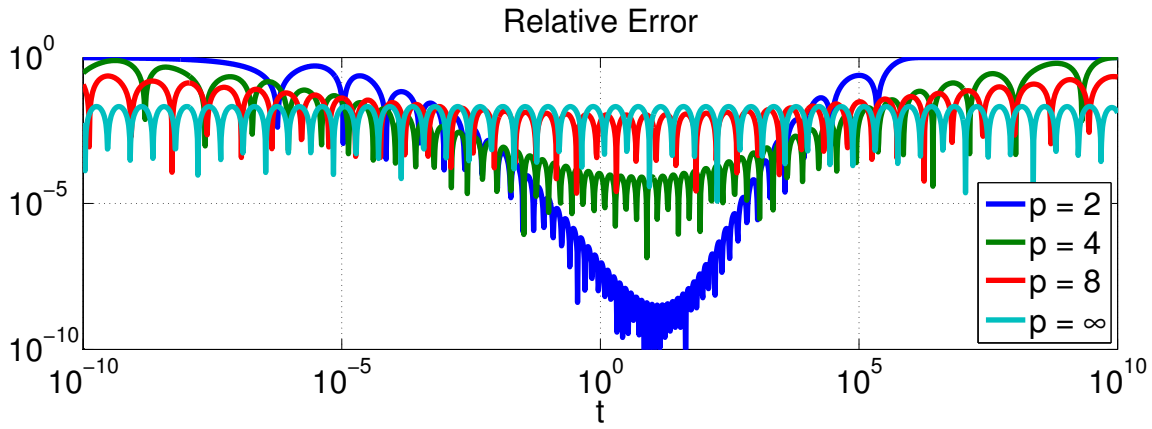

Fig. 3.1: The relative error for $K_\alpha^M(t)$ defined by equation (3.2) for $\alpha = 0.5$, using $M = 25$ Jacobi points, and several values of the scaling parameter p. For $p = \infty$, the method of Section 3.7 is used, with the same number of points.

A discretization of (3.3) with $M = 25$ points is also shown in Figure 3.1. The details of this discretization can be found below in Section 3.7. We observe that this latter representation will have uniform relative accuracy as a function of t, which (as we will see below) produces a better approximation for the fractional derivative than the Gauss-Jacobi quadrature. This point has been observed, and studied extensively by Beylkin and Monzón [2].

3.2 A quadrature rule with uniform relative accuracy

Motivated by the results in Figure 3.1, we next turn our attention to the mapping (3.3), which could have been obtained by directly substituting $y = \exp(z)$ into the original expression for the fractional kernel (2.1). Not only does this latter expression have the advantage that we no longer need to introduce (and make an optimal choice for) the scaling parameter p; it also turns out that we can discretize this integral with exponential accuracy using the trapezoidal rule to obtain a finite sum of exponentials from (3.3) in 3 principal steps:

1. Discretize the integral using the trapezoidal rule (Section 3.3).
2. Truncate the upper (Section 3.4) and lower (Section 3.5) limits of the sum.
3. Compress the first few terms using Gaussian quadrature (Section 3.6).

To simplify the presentation, which is very similar to that of Beylkin and Monzón [2], we restrict our attention to a relevant time interval, say $[\Delta t, T]$, and rescale the kernel. Defining the number of time steps $N = \lceil T/\Delta t \rceil$, we observe that the relative accuracy can be studied simply as a number of time steps, without specifying Δt. That is, we seek an approximation which achieves uniform relative accuracy ϵ, so that

$$\Gamma(\alpha) n^{-\alpha} = \int_{-\infty}^{\infty} e^{\alpha(z+z_\ell) - n e^{z+z_\ell}} dz = \sum_{m=1}^{M} w_m e^{-y_m n} + \Gamma(\alpha) n^{-\alpha} \delta_n, \qquad 1 \le n \le N, \tag{3.4}$$

where z_ℓ is to be chosen below, and we will have $|\delta_n| \le \epsilon$ for each n.

3.3 Discretization

We now discretize (3.3) with the trapezoidal rule, with step size $h > 0$. The error term can be obtained via the Poisson summation formula, so that

$$\Gamma(\alpha) n^{-\alpha} = h \sum_{-\infty}^{\infty} e^{\alpha(z_\ell + mh) - n e^{z_\ell + mh}} - \epsilon(n), \tag{3.5}$$

where

$$\epsilon(n) = \sum_{k\neq 0} \left[n^{-(\alpha+2\pi ik/h)} e^{-2\pi ikz_\ell} \Gamma(\alpha + 2\pi ik/h) \right]. \tag{3.6}$$

At this point we depart from [2] by observing that this error term can be more accurately bounded using Stirling's approximation for the Gamma function with complex argument [13]

$$\begin{aligned} |\epsilon(n)| &\leq 2n^{-\alpha} \sum_{k=1}^{\infty} |\Gamma(\alpha + 2\pi ik/h)| \\ &\leq 2n^{-\alpha} \sum_{k=1}^{\infty} \sqrt{2\pi}(2\pi k/h)^{\alpha-1/2} e^{-\pi^2 k/h} \\ &= 2n^{-\alpha}(2\pi)^{\alpha} h^{1/2-\alpha} \sum_{k=1}^{\infty} k^{\alpha-1/2} e^{-\pi^2 k/h}. \end{aligned}$$

Thus, given a prescribed tolerance ϵ, we solve the nonlinear equation for h

$$\epsilon = \left(\frac{2(2\pi)^{\alpha}}{\Gamma(\alpha)} \right) \left[\sum_{k=1}^{\infty} \left(\frac{k}{h} \right)^{\alpha-1/2} \exp\left(-\frac{(k-1)\pi^2}{h} \right) \right] \exp\left(-\frac{\pi^2}{h} \right). \tag{3.7}$$

The terms in parentheses are independent of h, and those in square brackets depend weakly on h. Thus, the error decays exponentially $\epsilon \approx \exp(-\pi^2/h)$, as expected when applying the trapezoidal rule over an infinite interval to a function of exponential type. The error bound derived in [2] gives $\epsilon \approx \exp(-2\pi/h)$. This latter bound predicts a step size h which is smaller by a factor of $(2\pi)/(\pi^2) \approx 0.64$, leading to a quadrature rule with roughly 50% more nodes than is actually necessary to achieve relative accuracy ϵ. We thus observe that

$$h \approx \frac{\pi^2}{\log\left(\frac{1}{\epsilon}\right)}.$$

In practice, $h = \mathcal{O}(1)$ for $\epsilon \in [10^{-2}, 10^{-15}]$.

3.4 Upper truncation

Once we have determined h, the infinite sum (3.5) represents $K_\alpha(n)$, to within the desired relative accuracy ϵ over the real half-line. We next truncate the infinite sum, without loss of accuracy, which will depend on N.

Upon examining the dependence of the summand (3.5) on the index m, we see that for large $m > 0$, the terms decrease super-exponentially. We now choose a value of $z_r = z_\ell + M_2 h$, for which the summand may be safely discarded for $m > M_2$. This leads to the constraint that

$$h \sum_{m=M_2}^{\infty} e^{\alpha(z_\ell+mh) - ne^{z_\ell+mh}} \leq \Gamma(\alpha) n^{-\alpha} \epsilon,$$

which is the most conservative when $n = 1$, and can be safely truncated to

$$h \exp\left(\alpha z_r - e^{z_r}\right) \leq \Gamma(\alpha)\epsilon, \tag{3.8}$$

and solved to obtain z_r. We treat this value as an upper bound, and once we have determined z_ℓ, then M_2 is chosen as the maximum integer such that $z_\ell + M_2 h \leq z_r$ satisfying (3.8). Because of the double-exponential decay, we find that

$$z_r \approx \ln\left(\ln\left(\frac{1}{\epsilon}\right)\right).$$

3.5 Lower truncation and further compression

Likewise, as $m \to -\infty$, the summand (3.5) becomes exponentially small. This point, also observed in [2], can be exploited to further reduce the number of terms required to maintain uniform relative accuracy ϵ. We present a slightly modified form of this compression, in which the total number M of exponential terms is minimized using error balancing.

We now define the quantity z_ℓ so that the sum can be decomposed into a principle part, and a lower sum which contains infinitely many terms

$$h \sum_{m=-\infty}^{0} e^{\alpha(z_\ell+mh)-ne^{z_\ell+mh}} + h \sum_{m=1}^{M_2} e^{\alpha(z_\ell+mh)-ne^{z_\ell+mh}}.$$

If we choose the quantity $\exp(z_\ell)$ to be small enough, then the lower sum can be safely neglected altogether, albeit at the expense of increasing M_2. On the other hand, if z_ℓ is increased, then the lower sum makes a significant contribution to the total approximation. It turns out that this lower sum can be replaced, without loss of accuracy, by a small number of weights and nodes (ω_m, η_m), for $m = 1, \dots M_1$, so that

$$\left| h \sum_{m=-\infty}^{0} e^{\alpha(z_\ell+mh)-ne^{z_\ell+mh}} - \sum_{m=1}^{M_1} \omega_m e^{-\eta_m n} \right| = \Gamma(\alpha) n^{-\alpha} \epsilon. \tag{3.9}$$

This will result in a fully truncated sum of the desired form (3.4), with

$$\Gamma(\alpha) n^{-\alpha} = \sum_{m=1}^{M_1} \omega_m e^{-\eta_m n} + h \sum_{m=1}^{M_2} e^{\alpha(z_\ell+mh)-ne^{z_\ell+mh}} + \Gamma(\alpha) n^{-\alpha} \delta_n, \qquad |\delta_n| \le \epsilon. \tag{3.10}$$

We note that $M = M_1 + M_2$. Thus, two tasks remain. First, we seek a strategy to minimize M, the total number of exponentials, which will be based on balancing truncation errors of the two approximations. Secondly, we need to define the quadrature rule (ω_m, η_m) accordingly.

We observe that the difference (3.9) will be the largest when $n = N$, and so the quantity z_ℓ must be chosen such that Ne^{z_ℓ} is sufficiently small. When this is the case, we can safely perform a Taylor series expansion, and re-order sums to find

$$\begin{aligned} h \sum_{m=-\infty}^{0} e^{\alpha(z_\ell+mh)-Ne^{z_\ell+mh}} &= h \sum_{m=0}^{\infty} e^{\alpha(z_\ell-mh)} \sum_{k=0}^{\infty} \frac{\left(-Ne^{z_\ell-mh}\right)^k}{k!} \\ &= e^{\alpha z_\ell} h \sum_{k=0}^{\infty} \frac{(-Ne^{z_\ell})^k}{k!} \sum_{m=0}^{\infty} e^{-(\alpha+k)mh} \\ &= \sum_{k=0}^{\infty} \frac{(-1)^k}{k!} \mu_k, \end{aligned}$$

where

$$\mu_k = N^{-\alpha} \left(\frac{h(Ne^{z_\ell})^{k+\alpha}}{1 - e^{-(\alpha+k)h}} \right). \tag{3.11}$$

Likewise, the terms $z_m = \eta_m N$ will also be small, and upon expanding the desired sum we obtain

$$\sum_{m=1}^{M_1} \omega_m e^{-\eta_m N} = \sum_{m=1}^{M_1} \omega_m e^{-z_m} = \sum_{k=0}^{\infty} \sum_{m=1}^{M_1} \omega_m \frac{(-z_m)^k}{k!},$$

which reduces the difference (3.9) to

$$\left| \sum_{k=0}^{\infty} \frac{(-1)^k}{k!} \left(\mu_k - \sum_{m=1}^{M_1} \omega_m z_m^k \right) \right| = N^{-\alpha} \epsilon.$$

For a sufficiently large integer $K = 2M_1$, we can choose (ω_m, η_m) so that the first K terms vanish

$$\sum_{m=1}^{M_1} \omega_m z_m^k = \mu_k, \qquad k = 0, 1, \dots 2M_1 - 1, \tag{3.12}$$

and ensure that the remainder can be made small

$$\left| \sum_{k=K}^{\infty} \frac{(-1)^k}{k!} \left(\mu_k - \sum_{m=1}^{M_1} \omega_m z_m^k \right) \right| \leq \frac{\mu_K}{K!} = N^{-\alpha}\epsilon, \qquad K = 2M_1.$$

Note that this equation depends on both z_ℓ, and the quadrature points M_1. We can therefore solve a constrained optimization problem for the total number $M = M_1 + M_2 = M_1 + (z_r - z_\ell)/h$ of quadrature points required to maintain uniform relative accuracy ϵ:

$$\text{Minimize } M = M_1 + \frac{z_r - z_\ell}{h} \text{ subject to } \frac{h(Ne^{z_\ell})^{2M_1+\alpha}}{\left(1 - e^{-(\alpha+2M_1)h}\right)(2M_1)!} - \epsilon = 0. \tag{3.13}$$

Many methods exist to solve this problem. Herein, we use the classical method of Lagrange multipliers. That is, we treat both z_ℓ and M_1 as continuous variables, optimize the values, and then round M_1 to the nearest integer. In practice, we often find that $M_1 = 1$ or 2 suffices, and so we can estimate the size of z_ℓ, which will be negative, as

$$z_\ell \approx -\ln(N) - \frac{1}{2M_1 + \alpha} \ln\left(\frac{1}{\epsilon}\right).$$

Combining this with our estimates for h and z_r, the number of exponentials required to achieve accuracy ϵ over N time steps is

$$M \sim \mathcal{O}\left(\log\left(\frac{1}{\epsilon}\right) \left[\log(N) + \log\left(\frac{1}{\epsilon}\right) + \log\left(\log\left(\frac{1}{\epsilon}\right)\right) \right] \right). \tag{3.14}$$

Thus, for fixed ϵ, the number of nodes required is $M = \mathcal{O}(\log N)$.

3.6 Determination of the lower quadrature rule

Finally, it remains to solve the system of equations (3.12). This we accomplish in two steps, using the classical theory of Gaussian quadrature. The first step is to obtain the quadrature nodes z_m, and the weights ω_m are obtained afterward. We start with the existence of a positive measure μ over the real line which defines the sequence (3.11) as moments

$$\int z^k d\mu(z) = \mu_k, \qquad k = 0, 1, \ldots,$$

which in turn guarantees the existence of a quadrature rule (ω_m, z_m) satisfying (3.12). Thus, we can find a monic polynomial

$$Q(z) = z^{M_1} + x_{M_1-1} z^{M_1-1} + \ldots x_1 z + x_0, \tag{3.15}$$

whose roots are precisely the desired quantities $z_1, z_2, \ldots z_{M_1}$, and which is orthogonal to all lower monomials

$$\int z^k Q(z) d\mu(z) = \mu_{k+M_1} + \sum_{m=0}^{M_1-1} x_m \mu_{k+m} = 0, \qquad k = 0, \ldots M_1 - 1.$$

These orthogonality conditions can be expressed as a linear system with a Hankel matrix

$$\begin{pmatrix} \mu_0 & \mu_1 & \cdots & \mu_{M_1-1} \\ \mu_1 & \mu_2 & \cdots & \mu_{M_1} \\ \vdots & & \ddots & \vdots \\ \mu_{M_1-1} & \mu_{M_1} & \cdots & \mu_{2M_1-2} \end{pmatrix} \begin{pmatrix} x_0 \\ x_1 \\ \vdots \\ x_{M_1-1} \end{pmatrix} = \begin{pmatrix} -\mu_{M_1} \\ -\mu_{M_1+1} \\ \vdots \\ -\mu_{2M_1-1} \end{pmatrix}. \tag{3.16}$$

So, we first solve this linear system to find the coefficients of the polynomial. Then, the roots of this equation yield $z_k = N\eta_k$, and we divide by N to find the appropriate nodes η_k.

Table 3.1: The number M of terms required to achieve relative accuracy ϵ in equation (2.2).

ϵ	$\alpha = 0.1$	$\alpha = 0.3$	$\alpha = 0.5$	$\alpha = 0.7$	$\alpha = 0.9$
10^{-2}	19	26	30	33	35
10^{-6}	65	73	78	81	85
10^{-10}	112	120	127	131	135
10^{-14}	160	169	175	179	183

The second step is to compute the weights, which are a solution to the overdetermined Vandermonde system

$$\begin{pmatrix} 1 & \dots & 1 \\ z_1 & \dots & z_{M_1} \\ \vdots & \ddots & \vdots \\ z_1^{2M_1-1} & \dots & z_{M_1}^{2M_1-1} \end{pmatrix} \begin{pmatrix} w_1 \\ \vdots \\ w_{M_1} \end{pmatrix} = \begin{pmatrix} \mu_0 \\ \mu_1 \\ \vdots \\ \mu_{2M_1-1} \end{pmatrix}.$$

Equivalently, this system can be posed using the normal equations of the system, $Cw = b$, where

$$C_{ij} = \frac{1 - (z_i z_j)^{2M_1}}{1 - z_i z_j}, \qquad b_j = \sum_{p=0}^{2M_1-1} \mu_p z_j^p. \tag{3.17}$$

The solution to this system yields the weights.

3.7 Summary

We compute the quadrature (3.10) according to algorithm 3 given below. The union of the two rules provides the M terms (3.10). We have shown in Figure 3.1 the uniform error property of the corresponding rule, using $\Delta t = 10^{-10}$, $T = 10^{10}$, $\alpha = 0.5$, and choosing a value of ϵ which would result in $M = 25$ points. The error shown there corresponds to $\epsilon = 0.021$, with $M_1 = 1$ and $M_2 = 24$. The relationship

Algorithm 3 Construction of the exponential sum

Given Δt, T, and ϵ,

1: Set $N = \lceil T/\Delta t \rceil$.
2: Use (3.7) to find h.
3: Use (3.8) to find z_r.
4: Use (3.13) to find z_ℓ and $M_2 = \lfloor (z_r - z_\ell)/h \rfloor$.
5: Define the upper portion of the quadrature rule

$$y_m = \frac{e^{z_\ell + mh}}{\Delta t}, \quad w_m = h \frac{\sin(\pi\alpha)}{\pi} y_m^\alpha, \qquad m = 1, 2, \dots M_2.$$

6: Define the moments μ_k by (3.11). Solve the Hankel system (3.16) for $\mathbf{x}$, and define the polynomial (3.15). Obtain the roots $z_m = N\eta_m$.
7: Solve the Vandermonde system (3.17) for the weights w_m. Then define the lower portion of the quadrature rule

$$\eta_m = \frac{z_m}{N\Delta t}, \quad \omega_m = \frac{\sin(\pi\alpha)}{\pi \Delta t^\alpha} w_m, \qquad m = 1, 2, \dots M_1.$$

between M, ϵ and α is shown in Tables 3.1 and 3.2.

4 Numerical Example

We now illustrate our procedure by constructing fractional derivatives according to (2.4), (2.10), (2.13), for a few test functions of the form

$$u(t) = t^k, \quad k = 0.2 + 0.4\ell, \qquad \ell = 1, 2, \dots 10,$$

Table 3.2: The relative accuracy ϵ achieved for a fixed number M of terms in equation (2.2).

M	$\alpha = 0.1$	$\alpha = 0.3$	$\alpha = 0.5$	$\alpha = 0.7$	$\alpha = 0.9$
10	8.7×10^{-2}	2.6×10^{-1}	2.4×10^{-1}	2.4×10^{-1}	2.5×10^{-1}
20	1.1×10^{-2}	3.3×10^{-2}	6.3×10^{-2}	1.0×10^{-1}	1.5×10^{-1}
40	1.3×10^{-4}	5.9×10^{-6}	1.3×10^{-3}	2.6×10^{-3}	4.3×10^{-3}
80	4.9×10^{-8}	2.5×10^{-7}	6.7×10^{-7}	1.4×10^{-6}	2.7×10^{-6}
160	1.2×10^{-14}	6.2×10^{-13}	1.7×10^{-13}	4.2×10^{-13}	9.3×10^{-13}

Table 4.1: Convergence of the fractional derivative of $u(t) = t^k$, of order $\alpha = 0.5$, with $P = 1$.

	k	0.6	1.0	1.4	1.8	2.2	2.6	3.0	3.4	3.8	4.2
Δt	M	Rate of Convergence									
0.01	12	0.100	*	0.900	1.300	1.491	1.489	1.485	1.481	1.478	1.475
0.005	14	0.100	*	0.900	1.300	1.494	1.490	1.487	1.485	1.483	1.481
0.0025	17	0.100	*	0.900	1.300	1.494	1.492	1.491	1.490	1.489	1.487
0.00125	19	0.100	*	0.900	1.300	1.495	1.494	1.493	1.493	1.492	1.491
0.000625	22	*	*	*	*	*	*	*	*	*	*

Table 4.2: Convergence of the fractional derivative of $u(t) = t^k$, of order $\alpha = 0.5$, with $P = 2$.

	k	0.6	1.0	1.4	1.8	2.2	2.6	3.0	3.4	3.8	4.2
Δt	M	Rate of Convergence									
0.01	17	0.100	*	0.900	1.300	1.700	2.100	2.495	2.489	2.484	2.480
0.005	20	0.100	*	0.900	1.300	1.700	2.100	2.494	2.491	2.488	2.486
0.0025	24	0.100	*	0.900	1.300	1.700	2.100	2.496	2.494	2.493	2.491
0.00125	28	0.100	*	0.900	1.300	1.700	2.100	2.497	2.496	2.495	2.494
0.000625	32	*	*	*	*	*	*	*	*	*	*

Table 4.3: Convergence of the fractional derivative of $u(t) = t^k$, of order $\alpha = 0.5$, with $P = 3$.

	k	0.6	1.0	1.4	1.8	2.2	2.6	3.0	3.4	3.8	4.2
Δt	M	Rate of Convergence									
0.01	21	0.100	*	0.900	1.300	1.700	2.100	*	2.900	3.300	3.490
0.005	26	0.100	*	0.900	1.300	1.700	2.100	*	2.900	3.300	3.493
0.0025	31	0.100	*	0.900	1.300	1.700	2.100	*	2.900	3.300	3.496
0.00125	36	0.100	*	0.900	1.300	1.700	2.100	*	2.900	3.300	3.498
0.000625	41	*	*	*	*	*	*	*	*	*	*

with exact solutions $t^{k-\alpha}\Gamma(k+1)/\Gamma(k+1-\alpha)$. We choose the fractional order to be $\alpha = 0.5$, and compute the derivative using $P = 1, 2, 3$ in the update equations (2.8), (2.11).

We set the relative accuracy to be $\epsilon = \Delta t^{P+1}$, to ensure that the quadrature error is smaller than the discretization error due to time stepping. We record the number of exponentials M, and the rates of convergence in Tables 4.1-4.3. Absolute errors are measured in the infinity norm, up to time $T = 1$. It is quite clear that the rate of convergence is

$$r = \min\{P + 1 - \alpha, k - \alpha\},$$

as proven in Lemma 2.1. The only exception is the specific case when k is an integer, for which the method is exact provided $k \leq P$. Thus, we see that the method is exact for $k = 1$ in each case, and for $k = 3$ in the case that $P = 3$. Since the method is exact, there are no rates of convergence to report, hence the "*". Note that when $P > 1$, some care is required to achieve the expected order of accuracy, since derivatives up to order $u^{(P)}$ must be constructed, even for the first few time steps. We accomplish this by replacing $u(t)$ with a polynomial of degree P,

$$u(t) = \sum_{p=0}^{P} u^p \ell_p(t), \qquad 0 < t < P\Delta t.$$

As a result, $\phi_0(p\Delta t)$ and $\phi_m(p\Delta t)$ actually rely on future information $u(p\Delta t)$ for the first few time steps. Since the function $u(t)$ is explicitly known, this poses no great difficulty; however, it makes the first P time levels implicit when solving fractional differential equations.

4.1 Comparison with other Fast Methods

We now compare our method to [16] that developed fast algorithms for evaluating fractional integrals. To make a direct comparison with Figure 5 of [16], we display the absolute error in the fractional kernel for $t \in [10^{-10}, 10^{10}]$, for several values of α and Δt. The quadrature approach of [16] utilizes a stretched exponential mapping

$$t^{-\alpha} = \frac{1}{\Gamma(2-\alpha)} \int_0^\infty e^{-\eta^\gamma t}\, d\eta, \qquad \gamma = \frac{1}{1-\alpha},$$

and, as shown in Figure 1 of [16], which we replicate in the top row of Figure 4.1 herein, this makes for a very smooth integrand. However, as t and α vary, the stretched exponential decays across orders of magnitude for the new integration variable $\eta \in [10^{-3}, 10^4]$. Thus the nodes η_k must be placed across a large range of the η-axis to maintain accuracy that is uniform in time.

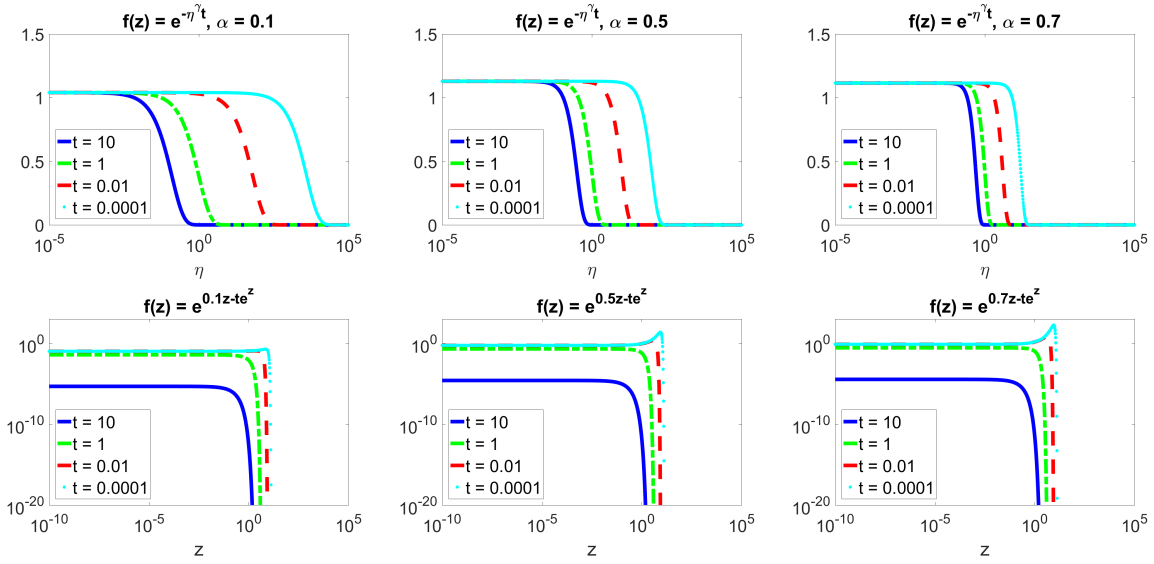

Fig. 4.1: The integrand (3.3) (bottom row) for various α and times t. When compared to Figure 1 of [16] (replicated here, top row), the dependence on t is more amenable.

By contrast, the double-exponential mapping (3.3) produces an integrand shown in the bottom row of Figure 4.1. Independent of t, the integrand is relatively flat for $z < 1$, which allows for dramatic reduction of the nodes z_k (i.e. kernel compression), without sacrificing accuracy. Furthermore, the range of z for which the integrand changes with respect to t is quite narrow, $z \in [10^{-1}, 10]$. As a result, we see that fewer nodes are required by an order of magnitude. This is further corroborated in Figure 4.2, which we offer in direct comparison to Figure 3 of [16].

We also solve the fractional integral problem for the function

$$f(t) = \frac{t}{1+t} + \sin(16.3t) + t^\alpha + t^{2\alpha} + t^{1+\alpha} + t^{2+2\alpha}, \tag{4.1}$$

used in [16], using our $P = 1$ method from (2.8), (2.11). The resulting error is shown in Figure 4.3, and behaves as depicted in the $p = 2$ case in Figure 4 of [16]; but here we require only 23 quadrature nodes to achieve the same accuracy. This would indicate that our method runs faster than that of [16] by an order of magnitude, with a dramatic reduction in storage.

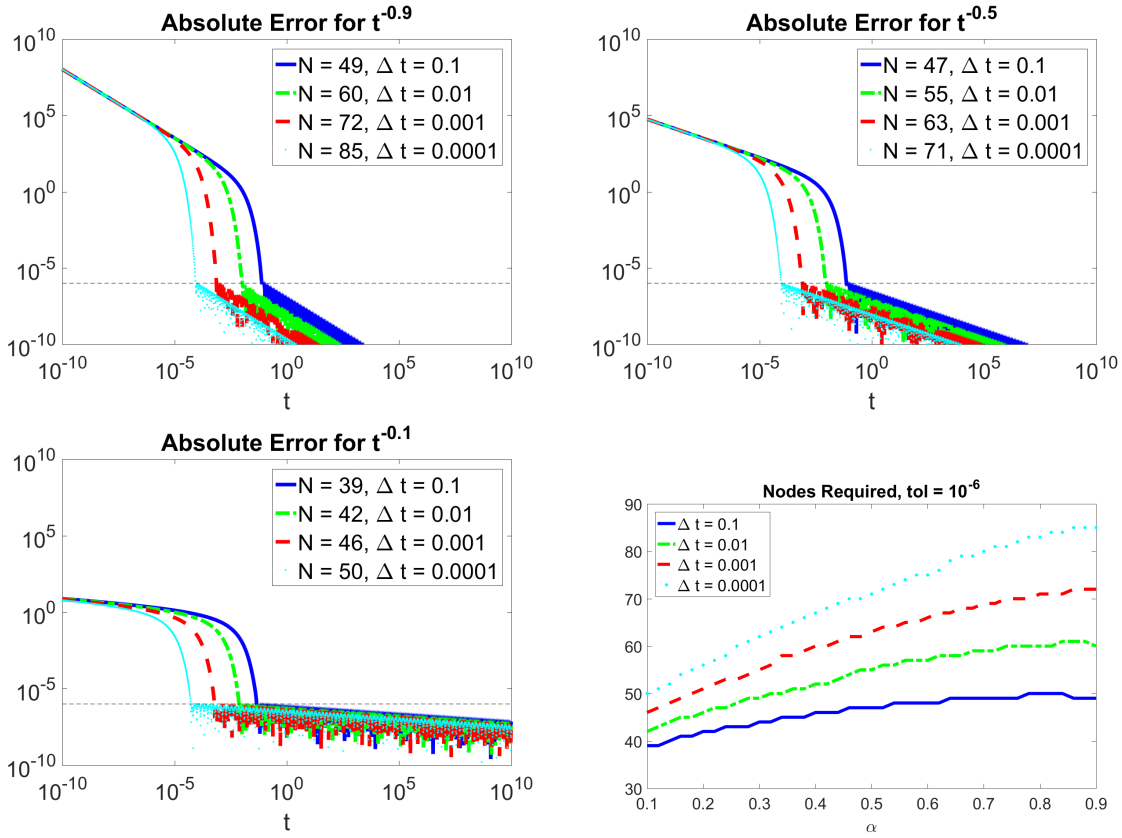

Fig. 4.2: The absolute error in approximating the fractional kernel $K(t) = t^{-\alpha}/\Gamma(1-\alpha)$, for various α and Δt. The current method reduces the number of nodes by an order of magnitude when compared to Figure 3 of [16].

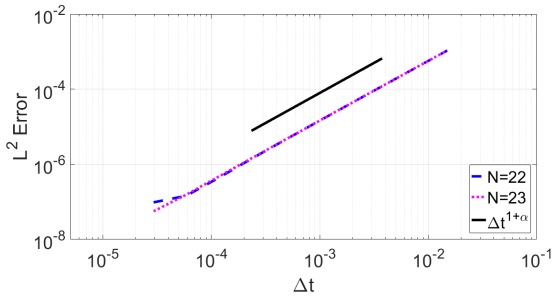

Fig. 4.3: The relative error in evaluating the fractional integral of (4.1), demonstrating that 23 quadrature nodes is sufficient to achieve second order accuracy.

5 Applications

Here we demonstrate the abilities of our solver to achieve high orders of accuracy, with relatively low computational cost.

5.1 The Kelvin-Voigt model of fractional relaxation

We first turn our attention to a problem popularized by Schmidt and Gaul [19]. We seek $x(t)$ satisfying the fractional Kelvin-Voigt model of viscoelasticity

$$cD_t^\alpha x + kx = f(t), \quad 0 < \alpha < 1, \quad t > 0, \tag{5.1}$$

with $c = 100$, $k = 10$, and $\alpha = 0.3$. In different contexts, this problem could also represent the Cole-Cole model of dielectric relaxation [6], or an intermediate variable in the fractional Zener model of viscoelasticity [15]. The right hand side function is $f(t) = f_0 = 1$ for $t > 0$, and 0 otherwise. The exact solution is then given in terms of the Mittag-Leffler function

$$x(t) = \frac{f_0}{k}\left(1 - E_\alpha\left(-\frac{kt^\alpha}{c}\right)\right). \tag{5.2}$$

Because $x(t) \to f_0/k\,(1 - \exp(-kt/c))$ as $\alpha \to 1$, equation (5.1) is sometimes referred to as a fractional

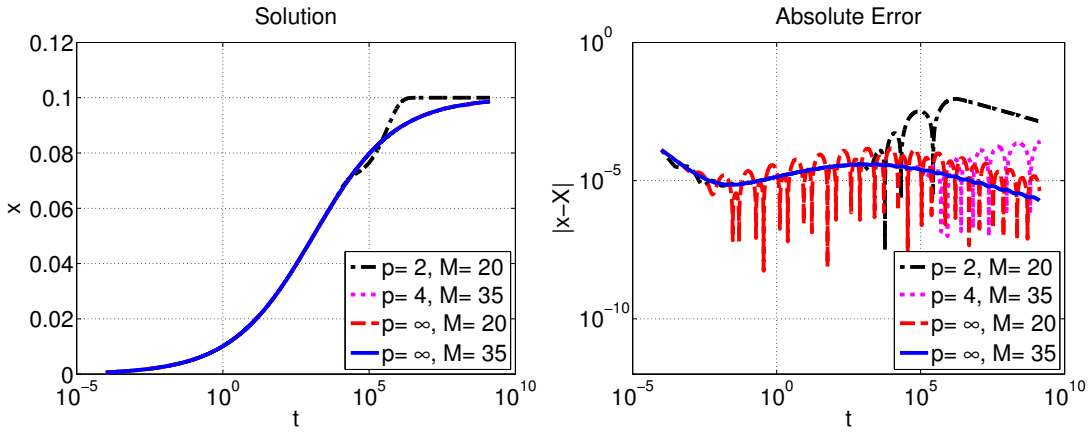

Fig. 5.1: Numerical solutions and the corresponding absolute errors for the Kelvin-Voigt problem (5.1). The number of quadrature points is denoted by M. When p is finite, Gauss-Jacobi quadrature (3.2) is used, otherwise the construction in Section 3.7 is used.

relaxation model. To make a direct comparison to other places in the literature [3,9], we solve the problem using the trapezoidal rule over a geometrically spaced set of grid points, as described in [9]. We note that the complexity of the algorithm is $O(MN)$. The numerical solution is constructed and illustrated in Figure 5.1 for $M = 20$ and $M = 35$, using Gauss-Jacobi quadrature and several choices of the scaling parameter p. As pointed out in [3], using $p = 4$ is advantageous over $p = 2$, but neither is able to deliver a pre-defined, uniform relative accuracy, as afforded by the exponential trapezoidal method ($p = \infty$) of Section 3.7 using $P = 1$. Notice that only with this latter method, and $M = 35$ quadrature points does the truncation error dominate the quadrature error due to the kernel approximation, thus producing a smooth error curve. In the $p = \infty$ case, the relative errors achieved by the quadrature are $\epsilon \approx 0.006$ and $\epsilon \approx 0.0008$ for $M = 20$ and $M = 35$, respectively.

We also measure the truncation error in the Kelvin-Voigt solution, with the same parameters, but over a uniform grid for $t \in (0, 5]$. Due to the discontinuous forcing function $f(t)$ employed the convergence rate of the proposed method depends heavily on the norm, and we observe that the order is as low as $\mathcal{O}(\Delta t^\alpha)$ in the infinity norm. For comparison in Table 5.1, we also solve the problem with the Green's function method proposed in [5], for which the step response is captured exactly, to within the numerical precision of the quadrature of the Green's function expansion. We first write the exact solution (5.2) as a convolution integral $x(t) = \chi(t) * f(t)$, where $\chi(t)$ is the derivative of the Mittag-Leffler function. Likewise, the numerical solution based on [5] is $X(t) = \chi_M(t) * f(t)$, where $\chi_M(t)$ is an M-term exponential sum approximation of χ. Upon taking the L^p norm over $t \in [0, T]$, it then immediately follows from Young's inequality that

$$\begin{aligned} ||x(t) - X(t)||_p &\le \|\chi(t) - \chi_M(t)\|_1 \, ||f||_p \\ &\le \|1\|_1 \, \|\chi(t) - \chi_M(t)\|_\infty \, ||f||_p \\ &\le \epsilon T ||f||_p. \end{aligned}$$

Table 5.1: Convergence of the Kelvin-Voight solution in three norms.

	Current Method						Ref. [5]					
	L^1		L^2		L^∞		L^1		L^2		L^∞	
Δt	Error	Rate	Error	Rate	Error	Rate	Error	Rate	Error	Rate	Error	Rate
0.016	4.0×10^{-3}	*	7.8×10^{-3}	*	5.4×10^{-2}	*	3.9×10^{-6}	*	1.9×10^{-6}	*	1.6×10^{-6}	*
0.008	2.1×10^{-3}	0.92	4.8×10^{-3}	0.68	4.7×10^{-2}	0.21	5.9×10^{-6}	*	2.7×10^{-6}	*	2.3×10^{-6}	*
0.004	1.1×10^{-3}	0.94	3.0×10^{-3}	0.69	4.1×10^{-2}	0.22	5.9×10^{-6}	*	2.7×10^{-6}	*	2.3×10^{-6}	*
0.002	5.8×10^{-4}	0.94	1.8×10^{-3}	0.71	3.5×10^{-2}	0.23	5.9×10^{-6}	*	2.8×10^{-6}	*	2.5×10^{-6}	*
0.001	3.0×10^{-4}	0.95	1.1×10^{-3}	0.72	3.0×10^{-2}	0.24	6.0×10^{-6}	*	2.8×10^{-6}	*	2.5×10^{-6}	*
0.0005	1.5×10^{-4}	0.96	6.7×10^{-4}	0.73	2.5×10^{-2}	0.25	6.0×10^{-6}	*	2.8×10^{-6}	*	2.5×10^{-6}	*
0.00025	8.2×10^{-5}	0.90	4.0×10^{-4}	0.74	2.1×10^{-2}	0.26	3.9×10^{-6}	*	1.9×10^{-6}	*	2.0×10^{-6}	*

5.2 Time-domain pulse propagation in a Cole-Cole dielectric

Next, we consider a source-free half-space $x > 0$, filled with a nonmagnetic ($\mu = \mu_0$) dielectric material whose relative permittivity is given in the frequency domain by the Cole-Cole model [6]

$$\hat{\epsilon}(i\omega) = \epsilon_\infty + \hat{\chi}(i\omega) = \epsilon_\infty + \frac{\epsilon_s - \epsilon_\infty}{1 + (i\omega\tau)^\alpha}. \tag{5.3}$$

The four parameters in (5.3) include the static (ϵ_s) and infinite-frequency (ϵ_∞) relative permittivities satisfying $1 \le \epsilon_\infty < \epsilon_s$; the characteristic relaxation time τ; and the fractional parameter $\alpha \in (0, 1)$. The Cole-Cole model simplifies to the Debye model [8] of exponential dielectric relaxation when $\alpha = 1$.

We will assume that the fields are zero for $t < 0$, and that at $t = 0$ an electric pulse $f(t)$ is introduced at the $x = 0$ boundary of the half-space. The geometry of the model problem reduces the magnetic, electric, and induced polarization field vectors to the scalar field quantities $H = H_y$, $E = E_z$, and $\mathcal{P} = \mathcal{P}_z$ respectively, so the corresponding signaling problem for the Maxwell system in $x \ge 0$ becomes

$$\frac{\partial}{\partial t}(\mu_0 H) = \frac{\partial E}{\partial x}, \tag{5.4}$$

$$\frac{\partial}{\partial t}(\epsilon_0 \epsilon_\infty E + \mathcal{P}) = \frac{\partial H}{\partial x}, \tag{5.5}$$

$$E(0, t) = f(t), \quad t \ge 0, \tag{5.6}$$

where ϵ_0 is the permittivity of free space. In the frequency domain $\hat{\mathcal{P}}(i\omega) = \epsilon_0 \hat{\chi}(i\omega)\hat{E}(i\omega)$, where $\hat{\chi}(i\omega)$ is the dielectric susceptibility. After algebraic manipulation and using the inverse Fourier transform to return to the time-domain, we arrive at a fractional differential equation of order α,

$$\tau^\alpha D_t^\alpha \mathcal{P} + \mathcal{P} = \epsilon_0(\epsilon_s - \epsilon_\infty)E, \quad \mathcal{P}(x, 0) = 0. \tag{5.7}$$

The Maxwell system (5.4)-(5.6) closed with the polarization law (5.7) constitutes the model problem whose numerical solution we seek. Before discretization of equations (5.4)-(5.5) and (5.7) we non-dimensionalize the problem by introducing the scaled variables

$$E' = \frac{1}{\sqrt{\epsilon_0}}E, \quad \mathcal{P}' = \sqrt{\epsilon_0}\mathcal{P}, \quad H' = \frac{1}{\sqrt{\mu_0}}H, \quad t' = \frac{t}{T_p}, \quad x' = \frac{\sqrt{\epsilon_0\mu_0}}{T_p}x. \tag{5.8}$$

The natural choice for the time scaling parameter would be $T_p = \tau$, but we retain a dimensionless parameter τ to provide a more general presentation of the model. Maxwell's equations are solved using the standard staggered Yee scheme. We denote the discrete electric field as $E_m^n = E(m\Delta x, n\Delta t)$, and similarly define the magnetic and polarization field. Inserting the scaled variables (5.8) and dropping the primes, we have

$$\frac{1}{\Delta t}\left(H_{m+\frac{1}{2}}^{n+\frac{1}{2}} - H_{m+\frac{1}{2}}^{n-\frac{1}{2}}\right) = \frac{1}{\Delta x}\left(E_{m+1}^n - E_m^n\right), \tag{5.9}$$

$$\frac{1}{\Delta t}\left(\epsilon_\infty(E_m^{n+1} - E_m^n) + \mathcal{P}_m^{n+1} - \mathcal{P}_m^n\right) = \frac{1}{\Delta x}\left(H_{m+\frac{1}{2}}^{n+\frac{1}{2}} - H_{m-\frac{1}{2}}^{n+\frac{1}{2}}\right). \tag{5.10}$$

The dimensionless infinite frequency speed $c_\infty = 1/\sqrt{\epsilon_\infty}$ defines the CFL number $\nu = c_\infty \frac{\Delta t}{\Delta x}$. The polarization law (5.7) is likewise discretized, using the local (2.10) and history (2.13) updates for the fractional derivative up to second order

$$\sum_{p=0}^{2} A_p \mathcal{P}_m^{n+1-p} + \tau^\alpha \sum_{j=1}^{N} w_j \phi_{jm}^{n+1} + \mathcal{P}_m^{n+1} = (\epsilon_s - \epsilon_\infty) E_m^{n+1}, \tag{5.11}$$
$$\phi_{jm}^{n+1} = d_j \phi_{jm}^n + c_j \left(\mathcal{P}_m^n - \mathcal{P}_m^{n-1} \right), \qquad j = 1, 2, \cdots N,$$

with coefficients

$$A_0 = \frac{(4-\alpha)h^{-\alpha}}{2\Gamma(3-\alpha)}, \quad A_1 = \frac{-2h^{-\alpha}}{\Gamma(3-\alpha)}, \quad A_2 = \frac{\alpha h^{-\alpha}}{2\Gamma(3-\alpha)}, \qquad h = \frac{\Delta t}{\tau}, \tag{5.12}$$

and

$$d_j = e^{-y_j \Delta t}, \quad c_j = \frac{e^{-y_j \Delta t}(1 - e^{-y_j \Delta t})}{y_j \Delta t}. \tag{5.13}$$

We identify the local coefficients with $P = 2$, and for comparative purpose consider the less accurate case of $P = 1$, where the coefficients will be

$$A_0 = \frac{h^{-\alpha}}{\Gamma(2-\alpha)}, \quad A_1 = \frac{-h^{-\alpha}}{\Gamma(2-\alpha)}, \quad A_2 = 0. \tag{5.14}$$

We observe that in both cases, $A_0 + A_1 + A_2 = 0$, a fact that will be used below. Because the polarization law (5.7) is discretized at $t = (n+1)\Delta t$, E and $\mathcal{P}$ are implicitly coupled. We next study the stability and phase error of this model, and prove that the FDTD method is convergent, with standard CFL condition $\nu \leq 1$.

5.2.1 Stability analysis

In the Von-Neumann stability framework [20] we let

$$H_{m+1/2}^{n+1/2} = H g^n e^{ikm\Delta x}, \quad E_m^n = E g^n e^{ikm\Delta x}, \quad \mathcal{P}_m^n = \mathcal{P} g^n e^{ikm\Delta x}, \quad \phi_{jm}^n = \phi_j g^n e^{ikm\Delta x},$$

and study the amplification factors g_ℓ by forming the $N+4$-dimensional linear system

$$G_1 g \mathbf{u} = G_0 \mathbf{u}, \quad \mathbf{u} = \left(H, \epsilon_\infty E, \mathcal{P}, \frac{\mathcal{P}}{g}, \phi_1, \ldots, \phi_N \right)^T.$$

Note that since 3 time levels of $\mathcal{P}$ explicitly appear in the equations, the inclusion of $\mathcal{P}/g$ as a component of $\mathbf{u}$ allows us to reduce the problem to a first order system. Due to the structure of the equations, we can analytically find G_1^{-1}, and turn the generalized eigenvalue problem into an ordinary one, namely $G\mathbf{u} = g\mathbf{u}$, where the structure is given by

$$G = \begin{pmatrix} A_{4\times 4} & B_{4\times N} \\ C_{N\times 4} & D_{N\times N} \end{pmatrix}$$

with submatrices given by outer products of the coefficient vectors $\mathbf{w}$, $\mathbf{c}$ and $\mathbf{d}$ (5.13),

$$A_{4\times 4} = \begin{pmatrix} 1 & \lambda/\epsilon_\infty & 0 & 0 \\ \lambda - \kappa\lambda & \mu - \kappa\mu & \delta - \gamma & \gamma \\ \kappa\lambda & \kappa\mu & 1 - \delta + \gamma & -\gamma \\ 0 & 0 & 1 & 0 \end{pmatrix}, \quad B_{4\times N} = \begin{pmatrix} 0 \\ \delta\tau^\alpha \\ -\delta\tau^\alpha \\ 0 \end{pmatrix} * \mathbf{w}^T,$$
$$C_{N\times 4} = \mathbf{c} * (\kappa\lambda, \kappa\mu, -1, 1), \quad D_{N\times N} = \mathrm{diag}(d_1, \ldots d_N),$$

and where additional coefficients are defined by

$$\delta = \frac{1}{r + A_0}, \qquad \gamma = (A_2 - \mathbf{w}^T \mathbf{c})\delta, \qquad \kappa = (r-1)\delta,$$
$$\lambda = 2i \frac{\Delta t}{\Delta x} \sin\left(\frac{k\Delta x}{2} \right), \quad \mu = 1 + \frac{\lambda^2}{\epsilon_\infty} = 1 - 4\nu^2 \sin^2\left(\frac{k\Delta x}{2} \right).$$

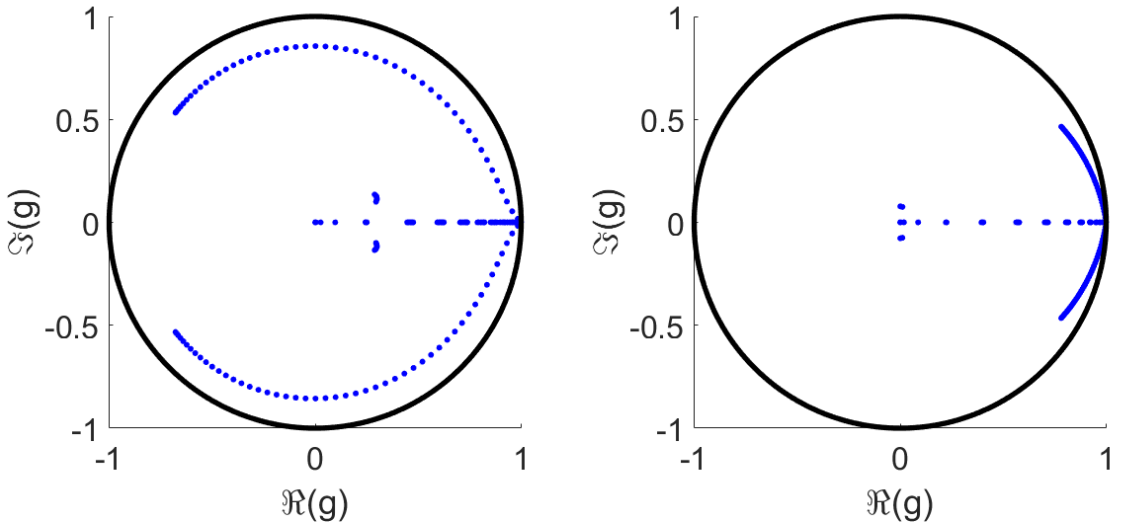

Fig. 5.2: Scatter plot of the amplification factors for varying k satisfying $0 < k\Delta x < \pi$. As k increases, the 2 propagating modes traverse arcs within the unit disk, and the remaining $N + P + 1$ roots remain largely unchanged. The pertinent parameters are $r = 75$, $\Delta t = 10^{-3}\tau$ and $\alpha = 0.75$ (left) and 0.25 (right).

The eigenvalues g_ℓ are studied numerically as a function of the wave number k, and a representative example is shown in Figure 5.2. The eigenvalues will consist of 2 principle roots, corresponding to wave propagation, and $N + P + 1$ spurious roots introduced by the polarization law and our approximation of the fractional derivative. We observe that the spurious roots are largely independent of k, and the propagating roots traverse an arc within the unit circle in the complex g plane, beginning at $g = 1$ when $k = 0$, and approaching $g = -1$ for $k = \pi$.

Theorem 5.1 *The numerical scheme* (5.9), (5.11) *is stable provided that the CFL number satisfies* $\nu = c_\infty \frac{\Delta t}{\Delta x} \leq 1$.

Proof We can focus on these principle roots by studying the stability polynomial as rational function. Indeed, the eigenvalues equivalently satisfy

$$\Phi(g) = (g-1)^2 \left(1 + \frac{r-1}{1+\sigma(g)}\right) + 4\nu^2 \sin^2\left(\frac{k\Delta x}{2}\right) g = 0, \tag{5.15}$$

where $\nu = c_\infty \Delta t/\Delta x$ is the CFL number. The main advantage to this approach is that now the fractional derivative approximation is characterized by $\sigma(g)$, and will therefore contain all of the information involving the exponential sum (5.13), as well as the local coefficients (5.12), or (5.14)

$$\sigma(g) = \left(1 - \frac{1}{g}\right)\left(A_0 - \frac{A_2}{g} + \tau^\alpha \sum_{j=1}^{N} \frac{w_j c_j}{g - d_j}\right). \tag{5.16}$$

Note that we have used the fact that $A_1 = -A_0 - A_2$ to factor out the $(1 - 1/g)$ term, and that when we take $P = 1$ (5.14), $A_2 = 0$. The stability condition will be the most restrictive in the regime where $k\Delta x \to \pi$, and $g \to -1$. If we set $k\Delta x = \pi$, and $g = -1$ in the expression for the fractional derivative, we arrive at a quadratic polynomial

$$\Phi(g) \approx (g-1)^2 \left(1 + \frac{r-1}{1+\sigma(-1)}\right) + 4\nu^2 g = 0.$$

Applying the Schur criterion [20], we have the following approximate stability condition

$$\nu^2 \leq 1 + \frac{r-1}{1 + 2(A_0 + A_2 - \rho)}, \quad \rho = \sum_{j=1}^{N} \frac{w_j c_j}{1 + e^{-y_j \Delta t}}. \tag{5.17}$$

But since this is an upper bound, it is sufficient to enforce the standard CFL condition $\nu^2 \leq 1$.

From numerical simulations using the proposed FDTD method, we have observed that instabilities can be suppressed for values of ν slightly greater than 1, in agreement with the upper bound (5.17). In Table 5.2, we record the actual onset of instabilities, with the values predicted by (5.17). The actual onset of the instability is approximated quite closely.

Table 5.2: Validation of Stability Conditions given by equation (5.17). The columns ν_{Actual} are obtained by running FDTD simulations and observing instabilities.

	P=1		P=2	
$\frac{\Delta t}{\tau}$	$\nu_{Predicted}$	ν_{Actual}	$\nu_{Predicted}$	ν_{Actual}
0.001	1.1013	1.1013	1.0616	1.0601
0.0001	1.0188	1.0188	1.0113	1.0112
0.00001	1.0034	1.0034	1.0021	1.0020

The stability conditions can be reformulated in dimensional quantities; replacing the CFL condition and rearranging, the stability conditions take the form

$$\left(\frac{c\Delta t}{\Delta x}\right)^2 \leq \left(\epsilon_\infty + \frac{\epsilon_s - \epsilon_\infty}{1 + \sigma(-1)}\right), \tag{5.18}$$

where $c = 1/\sqrt{\epsilon_0 \mu_0}$, and the right hand side is an approximation to ϵ_∞. It can be shown that $\sigma(-1) = O(\Delta t^{-\alpha})$, so we only recover the true infinite frequency limit when $\Delta t \to 0$. Thus, in principal we can exceed the traditional CFL limit by a small amount, as indicated in Table 5.2. This is due to the fact that the maximum wave speed c_∞ is not supported by the propagation, as the quadrature used in the fractional derivative cannot accurately resolve the infinite frequency limit of the permittivity. But as Δt decreases, this distinction becomes negligible. So in practice we take $\nu = 1$, which is sufficient if not necessary to maintain stability.

5.2.2 Phase error analysis

The phase error represents the total error in the system (5.9) for a given spatial Fourier component $k = k(\omega)$. It will be composed of the truncation error due to discretizing the PDEs, as well as the quadrature error in approximating the fractional derivative. We examine the phase error $\Phi_{N,h} = |k_{N,h}/k - 1|$ for a given value of α by varying both N and $h = \Delta t/\tau$, for $\omega \Delta t \leq \pi$. The wave number k is given by

$$k^2 = \omega^2 \mu_0 \epsilon_0 \left(\epsilon_\infty + \frac{\epsilon_s - \epsilon_\infty}{1 + (i\omega\tau)^\alpha}\right) = \left(\frac{\omega}{c}\right)^2 (\epsilon_\infty + \hat{\chi}). \tag{5.19}$$

The discretized wave number similarly satisfies

$$\frac{4}{\Delta x^2} \sin^2\left(\frac{k_{N,h}\Delta x}{2}\right) = \frac{4}{(c_\infty \Delta t)^2} \sin^2\left(\frac{\omega \Delta t}{2}\right) \left(1 + \frac{r-1}{1 + \sigma\left(e^{i\omega\Delta t}\right)}\right), \tag{5.20}$$

where $\sigma\left(e^{i\omega\Delta t}\right) \approx (i\omega\tau)^\alpha$ is an approximation of the fractional derivative, as shown in the stability analysis. This approximation is of the form

$$\sigma\left(e^{i\omega\Delta t}\right) = \left(1 - e^{-i\omega\Delta t}\right) \left(A_0 - A_2 e^{-i\omega\Delta t} + \sum_{j=1}^{N} \frac{w_j c_j e^{-i\omega\Delta t}}{1 - e^{-(y_j + i\omega)\Delta t}}\right). \tag{5.21}$$

As in the stability analysis, we have again made use of the fact that $A_1 = -A_0 - A_2$ to eliminate one of the coefficients.

For frequencies ω satisfying $\omega \Delta t \ll 1$, we can study the order of convergence in the phase error. We observe that

Theorem 5.2 *The solutions of the FDTD scheme (5.9), (5.11) will have a phase error that is $O(\Delta t^2)$ for $\omega \Delta t \ll 1$.*

Proof First, note that

$$c_j = e^{-y_j \Delta t} \frac{1 - e^{-y_j \Delta t}}{y_j \Delta t} = \frac{e^{-y_j \Delta t}}{\Delta t} \int_0^{\Delta t} e^{-y_j u} du, \quad j = 1, 2, \ldots N, \tag{5.22}$$

and that according to equation (2.2), the sums involving exponentials will satisfy

$$\sum_{j=1}^{N} w_j e^{-y_j \Delta t} \approx K_\alpha(\Delta t) = \frac{\Delta t^{-\alpha}}{\Gamma(1-\alpha)}, \tag{5.23}$$

with a small error ϵ. The denominator of (5.21) can be expanded as an infinite series, and using the coefficients (5.14), we find that

$$\begin{aligned}
\sigma\left(e^{i\omega\Delta t}\right) &= \frac{1 - e^{-i\omega\Delta t}}{\Delta t} \left(\frac{\Delta t^{1-\alpha}}{\Gamma(2-\alpha)} + \sum_{n=0}^{\infty} \sum_{j=1}^{N} w_j \int_0^{\Delta t} e^{-(n+1)(y_j + i\omega)\Delta t - y_j u} du \right) \\
&= \frac{1 - e^{-i\omega\Delta t}}{\Delta t} \left(\frac{\Delta t^{1-\alpha}}{\Gamma(2-\alpha)} + \sum_{n=1}^{\infty} e^{-ni\omega\Delta t} \int_{n\Delta t}^{(n+1)\Delta t} \sum_{j=1}^{N} w_j e^{-y_j u} du \right) \\
&= \frac{1 - e^{-i\omega\Delta t}}{\Delta t} \sum_{n=0}^{\infty} e^{-ni\omega\Delta t} \int_{n\Delta t}^{(n+1)\Delta t} \frac{u^{-\alpha}}{\Gamma(1-\alpha)} du,
\end{aligned} \tag{5.24}$$

where in the final step, we have used the fact that A_0 is clearly the $n = 0$ contribution to the summand. If we observe that

$$\frac{1 - e^{-i\omega\Delta t}}{\Delta t} e^{-ni\omega\Delta t} = e^{-i\omega u} + O((\omega\Delta t)^2), \quad n\Delta t \le u \le (n+1)\Delta t, \tag{5.25}$$

then it follows that the fractional derivative will have a second order error

$$\sigma\left(e^{i\omega\Delta t}\right) = (i\omega\tau)^\alpha + O((\omega\Delta t)^2), \tag{5.26}$$

and substitution into the phase shows that the phase error will also be second order in both cases. An analogous argument is made for the $P = 2$ case, but with the first two terms of the summand (5.21) coming from the local expansion coefficients (5.12).

5.3 Numerical results

The solution to the system (5.9)-(5.14) was computed for $\alpha = 0.6$ and 0.75, with the remaining parameters fixed and scaled according to (5.8). We take $\epsilon_s = 75, \epsilon_\infty = 1, \tau = 1$ and the CFL condition is $\nu = 1$.

Table 5.3: $\alpha = 0.4$, $q = 1$.

	$x = 0.008$		$x = 0.016$		$x = 0.024$		$x = 0.032$		$x = 1$		$x = 5$		$x = 10$		$x = 15$	
Δt	Error	Rate	Error	Rate	Error	Rate	Error	Rate	Error	Rate	Error	Rate	Error	Rate	Error	Rate
0.008	1.96E-02	*	1.26E-02	*	1.58E-02	*	1.03E-02	*	5.69E-04	*	6.69E-05	*	2.51E-05	*	1.43E-05	*
0.004	9.91E-03	0.99	4.21E-03	1.36	6.14E-03	1.58	3.11E-03	1.72	1.32E-04	2.11	1.55E-05	2.11	5.81E-06	2.11	3.30E-06	2.11
0.002	3.83E-03	1.37	1.11E-03	1.75	1.83E-03	1.93	7.70E-04	2.01	2.95E-05	2.16	3.46E-06	2.16	1.30E-06	2.16	7.37E-07	2.16
0.001	1.12E-03	1.77	2.50E-04	2.07	4.36E-04	2.15	1.70E-04	2.18	6.25E-06	2.24	7.29E-07	2.25	2.73E-07	2.25	1.55E-07	2.25
0.0005	2.57E-04	2.13	5.06E-05	2.27	9.03E-05	2.30	3.41E-05	2.32	1.19E-06	2.40	*	*	*	*	*	*
0.00025	4.86E-05	2.40	8.69E-06	2.50	1.60E-05	2.54	5.74E-06	2.57	1.74E-07	2.77	*	*	*	*	*	*
0.000125	7.05E-06	2.78	9.36E-07	3.04	1.94E-06	3.21	5.63E-07	3.35	3.97E-09	5.45	*	*	*	*	*	*

The electric field was prescribed at $x = 0$ to be a unit impulse of duration $T_p = \tau = 1$ and amplitude $1/T_p = 1$. The signal was recorded up to time $T = 250\tau$, and a depth of $L = 20 c_\infty \tau$. The resulting time trace was recorded at a shallow, medium and large spatial depths, as illustrated in Figure 5.3. Also shown in Tables 5.3-5.8 are the L^2 relative errors $||E_{exact} - E||_{t\in[0,T]} / ||E_{exact}||_{t\in[0,T]}$, for several levels of refinement of Δt. The exact solution is obtained by the inverse Laplace transform method, as constructed in [4]. We notice that in this case we verify the expected convergence rates for the two values of q employed, even though our signaling data (5.6) is discontinuous. A mathematical property of

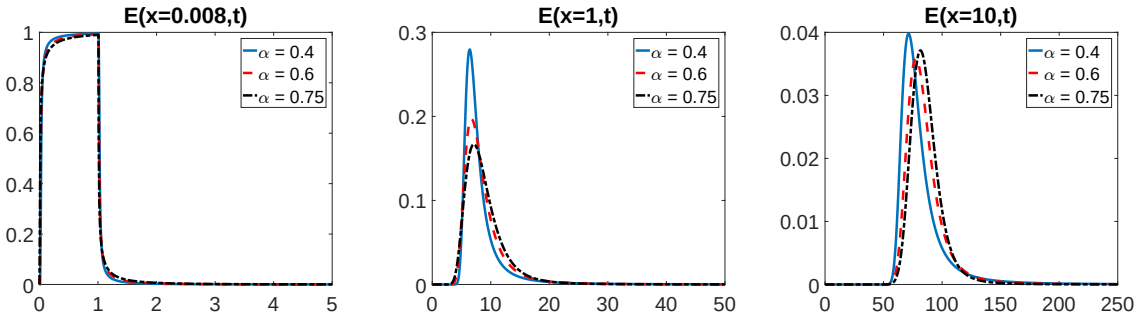

Fig. 5.3: Plot of the electric field due to a step pulse of duration $T_p = \tau$, at short ($x = 0.008 c_\infty \tau$), medium ($x = c_\infty \tau$), and large ($x = 10 c_\infty \tau$) depths. The initial waveform is present only at short depths, and the value of α effects the symmetry of the pulse, as well as the rate of attenuation.

Table 5.4: $\alpha = 0.4$, $q = 2$.

	$x = 0.008$		$x = 0.016$		$x = 0.024$		$x = 0.032$		$x = 1$		$x = 5$		$x = 10$		$x = 15$	
Δt	Error	Rate	Error	Rate	Error	Rate	Error	Rate	Error	Rate	Error	Rate	Error	Rate	Error	Rate
0.008	1.97E-02	*	1.30E-02	*	1.61E-02	*	1.08E-02	*	6.89E-04	*	8.18E-05	*	3.08E-05	*	1.75E-05	*
0.004	1.00E-02	0.97	4.64E-03	1.30	6.51E-03	1.49	3.53E-03	1.61	1.72E-04	2.00	2.05E-05	2.00	7.70E-06	2.00	4.38E-06	2.00
0.002	4.07E-03	1.30	1.37E-03	1.61	2.14E-03	1.76	9.89E-04	1.84	4.31E-05	2.00	5.12E-06	2.00	1.92E-06	2.00	1.10E-06	2.00
0.001	1.35E-03	1.59	3.66E-04	1.83	6.02E-04	1.91	2.57E-04	1.95	1.08E-05	2.00	1.28E-06	2.00	4.81E-07	2.00	2.74E-07	2.00
0.0005	3.84E-04	1.81	9.32E-05	1.94	1.57E-04	1.97	6.49E-05	1.98	2.70E-06	2.00	*	*	*	*	*	*
0.00025	1.01E-04	1.93	2.34E-05	1.98	3.97E-05	1.99	1.63E-05	2.00	6.74E-07	2.00	*	*	*	*	*	*
0.000125	2.57E-05	1.98	5.87E-06	1.99	9.98E-06	2.00	4.07E-06	2.00	1.68E-07	2.00	*	*	*	*	*	*

Table 5.5: $\alpha = 0.6$, $q = 1$.

	$x = 0.008$		$x = 0.016$		$x = 0.024$		$x = 0.032$		$x = 1$		$x = 5$		$x = 10$		$x = 15$	
Δt	Error	Rate	Error	Rate	Error	Rate	Error	Rate	Error	Rate	Error	Rate	Error	Rate	Error	Rate
0.008	1.09E-02	*	4.66E-03	*	7.16E-03	*	3.22E-03	*	9.10E-05	*	1.32E-05	*	6.15E-06	*	4.04E-06	*
0.004	5.50E-03	0.98	1.13E-03	1.63	2.32E-03	2.05	6.24E-04	2.37	1.84E-06	5.63	1.10E-07	6.91	4.53E-08	7.09	2.98E-08	7.09
0.002	2.30E-03	1.26	2.56E-04	1.86	6.39E-04	2.14	1.44E-04	2.12	8.15E-06	-2.15	1.27E-06	-3.53	6.01E-07	-3.73	3.98E-07	-3.74
0.001	9.00E-04	1.36	1.23E-04	1.48	2.30E-04	1.06	8.62E-05	0.74	5.19E-06	0.65	7.94E-07	0.67	3.75E-07	0.68	2.48E-07	0.68
0.0005	3.55E-04	1.34	6.27E-05	1.10	1.07E-04	0.97	4.43E-05	0.96	2.49E-06	1.06	*	*	*	*	*	*
0.00025	1.43E-04	1.31	2.83E-05	1.15	4.83E-05	1.15	1.99E-05	1.16	1.08E-06	1.21	*	*	*	*	*	*
0.000125	5.83E-05	1.29	1.19E-05	1.24	2.05E-05	1.25	8.31E-06	1.26	4.40E-07	1.29	*	*	*	*	*	*

Table 5.6: $\alpha = 0.6$, $q = 2$.

	$x = 0.008$		$x = 0.016$		$x = 0.024$		$x = 0.032$		$x = 1$		$x = 5$		$x = 10$		$x = 15$	
Δt	Error	Rate	Error	Rate	Error	Rate	Error	Rate	Error	Rate	Error	Rate	Error	Rate	Error	Rate
0.008	9.85E-03	*	5.46E-03	*	7.36E-03	*	4.28E-03	*	2.58E-04	*	3.88E-05	*	1.82E-05	*	1.20E-05	*
0.004	4.68E-03	1.07	1.73E-03	1.50	2.59E-03	1.66	1.27E-03	1.75	6.45E-05	2.00	9.69E-06	2.00	4.56E-06	2.00	3.01E-06	2.00
0.002	1.72E-03	1.45	4.93E-04	1.69	8.03E-04	1.81	3.45E-04	1.88	1.61E-05	2.00	2.42E-06	2.00	1.14E-06	2.00	7.52E-07	2.00
0.001	5.62E-04	1.61	1.32E-04	1.80	2.30E-04	1.90	8.97E-05	1.94	4.04E-06	2.00	6.06E-07	2.00	2.85E-07	2.00	1.88E-07	2.00
0.0005	1.73E-04	1.70	3.42E-05	1.88	6.26E-05	1.95	2.28E-05	1.98	1.01E-06	2.00	*	*	*	*	*	*
0.00025	5.14E-05	1.75	8.68E-06	1.94	1.63E-05	1.98	5.74E-06	1.99	2.52E-07	2.00	*	*	*	*	*	*
0.000125	1.44E-05	1.84	2.19E-06	1.97	4.16E-06	1.99	1.44E-06	1.99	6.31E-08	2.00	*	*	*	*	*	*

Table 5.7: $\alpha = 0.75$, $q = 1$.

	$x = 0.008$		$x = 0.016$		$x = 0.024$		$x = 0.032$		$x = 1$		$x = 5$		$x = 10$		$x = 15$	
Δt	Error	Rate	Error	Rate	Error	Rate	Error	Rate	Error	Rate	Error	Rate	Error	Rate	Error	Rate
0.008	1.41E-02	*	5.16E-03	*	8.28E-03	*	3.38E-03	*	9.38E-05	*	1.96E-05	*	1.09E-05	*	7.90E-06	*
0.004	1.01E-02	0.47	2.81E-03	0.85	4.61E-03	0.88	1.71E-03	0.98	6.57E-05	0.51	1.36E-05	0.53	7.56E-06	0.53	5.46E-06	0.53
0.002	6.39E-03	0.66	1.48E-03	0.71	2.82E-03	0.93	8.67E-04	0.98	3.42E-05	0.94	7.06E-06	0.95	3.92E-06	0.95	2.83E-06	0.95
0.001	3.66E-03	0.80	7.22E-04	0.83	1.59E-03	1.03	4.00E-04	1.12	1.60E-05	1.09	3.30E-06	1.10	1.83E-06	1.10	1.32E-06	1.10
0.0005	2.01E-03	0.87	3.25E-04	1.01	7.90E-04	1.15	1.75E-04	1.20	7.14E-06	1.16	*	*	*	*	*	*
0.00025	1.21E-03	0.73	1.38E-04	1.09	3.72E-04	1.23	7.48E-05	1.23	3.11E-06	1.20	*	*	*	*	*	*
0.000125	7.49E-04	0.70	5.79E-05	1.18	1.64E-04	1.26	3.18E-05	1.23	1.33E-06	1.22	*	*	*	*	*	*

the hyperbolic system in a Cole-Cole dielectric is that discontinuities, found on the characteristics, are infinitely smoothed out [17] hence our numerical results in this wave propagation experiment exhibit the expected convergence rates in contrast to the numerical experiment in Section 5.1. Similar accuracy and

Table 5.8: $\alpha = 0.75$, $q = 2$.

	$x = 0.008$		$x = 0.016$		$x = 0.024$		$x = 0.032$		$x = 1$		$x = 5$		$x = 10$		$x = 15$	
Δt	Error	Rate	Error	Rate	Error	Rate	Error	Rate	Error	Rate	Error	Rate	Error	Rate	Error	Rate
0.008	9.45E-03	*	3.70E-03	*	6.76E-03	*	2.57E-03	*	1.53E-04	*	3.14E-05	*	1.74E-05	*	1.25E-05	*
0.004	6.99E-03	0.44	1.26E-03	1.05	3.26E-03	1.55	8.33E-04	1.62	3.83E-05	2.00	7.84E-06	2.00	4.34E-06	2.00	3.13E-06	2.00
0.002	4.65E-03	0.59	5.13E-04	1.13	1.49E-03	1.30	2.89E-04	1.53	9.58E-06	2.00	1.96E-06	2.00	1.09E-06	2.00	7.84E-07	2.00
0.001	3.01E-03	0.63	2.36E-04	1.27	6.20E-04	1.12	9.09E-05	1.67	2.40E-06	2.00	4.90E-07	2.00	2.71E-07	2.00	1.96E-07	2.00
0.0005	1.82E-03	0.73	8.45E-05	1.12	2.85E-04	1.48	2.61E-05	1.80	5.99E-07	2.00	*	*	*	*	*	*
0.00025	9.77E-04	0.90	2.56E-05	0.98	1.45E-04	1.73	6.64E-06	1.98	1.50E-07	2.00	*	*	*	*	*	*
0.000125	4.44E-04	1.14	6.87E-06	1.40	5.47E-05	1.90	1.57E-06	2.08	3.74E-08	2.00	*	*	*	*	*	*

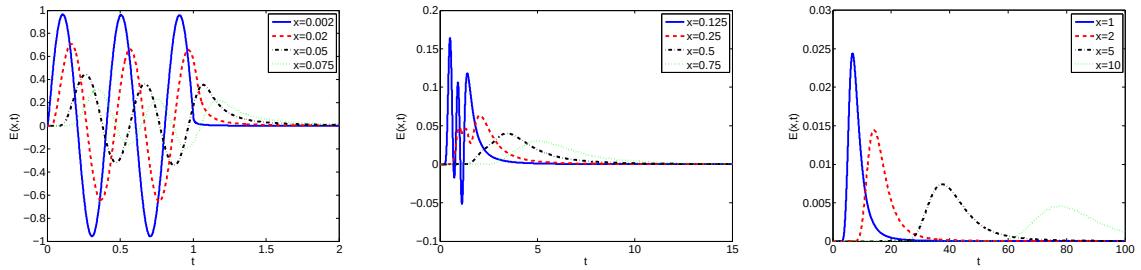

Fig. 5.4: Evolution of a sinuosoidal waveform through a Cole-Cole medium, with $\alpha = 0.5$. As high frequency content is attenuated, a characteristic pulse emerges at large depths.

convergence rates were observed with rectangular-pulse modulated sinusoid signaling data, whose time evolution at various depths in the medium is shown in Figure 5.4.

6 Conclusion

We have constructed a means to efficiently and accurately compute the Caputo fractional derivative in order to solve fractional differential equations that model constitutive laws in viscoelasticity and electromagnetics. The method relies on the kernel compression techniques shown in [2], along with several modifications introduced here to further reduce the computational burden. By further incorporating local time-stepping procedures up to some order $P \geq 1$, high accuracy can be afforded without losing efficiency. The application of this procedure to other fractional partial differential equations is the topic of our ongoing research.

References

1. K. Atkinson, *An Introduction to Numerical Analysis*, 2 ed., Wiley, 1989.
2. G. Beylkin and L. Monzón, *Approximation by exponential sums revisited*, Appl. Comput. Harmon. Anal. **28** (2010), no. 2, 131–149.
3. C. Birk and C. Song, *An improved non-classical method for the solution of fractional differential equations*, Computational Mechanics **46** (2010), no. 5, 721–734 (English).
4. M. F. Causley and P. G. Petropoulos, *On the time-domain response of havriliak-negami dielectrics*, IEEE TRANSACTIONS ON ANTENNAS AND PROPAGATION **61** (2013), no. 6, 3182–3189.
5. M. F. Causley, P. G. Petropoulos, and S. Jiang, *Incorporating the havriliak-negami dielectric model in the fdtd method*, J. Comp. Phys. **230** (2011), no. 10, 3884–3899.
6. K. S. Cole and R. H. Cole, *Dispersion and absorption in dielectrics i. alternating current characteristics*, J. Chem. Phys. **9** (1941), 341–52.
7. J. Cooper, B. Marx, J. Buhl, and V. Hombach, *Determination of safety distance limits for a human near a cellular base station antenna, adopting the ieee standard or icnirp guidelines*, Bioelectromagnetics **23** (2000), no. 6, 429–443.
8. P. Debye, *Polar molecules*, Chemical Catalogue Company, New York (1929).

9. K. Diethelm, *An investigation of some nonclassical methods for the numerical approximation of caputo-type fractional derivatives*, Numerical Algorithms (2008), 361–390.
10. C. Gabriel and S. Gabriel, *Compilation of the dielectric properties of body tissues at rf and microwave frequencies*, U.S.A.F Armstrong Lab., Brooks AFB, TX, Technical Rep. AL/OE-TR-1996-0037 (1996).
11. A. Hanyga and J.-F. Lu, *Wave field simulation for heterogeneous transversely isotropic porous media with the jkd dynamic permeability*, Computational Mechanics **36** (2005), 196–208.
12. S. Jiang and L. Greengard, *Fast evaluation of nonreflecting boundary conditions for the schrdinger equation in one dimension*, Computers Mathematics with Applications **47** (2004), no. 6-7, 955 – 966.
13. A. A. Kilbas and M. Saigo, *A remark on asymptotics of the gamma function at infinity (study on applications for fractional calculus operators in univalent function theory)*, RIMS Kokyuroku **1363** (2004), 33–36.
14. T. Kim, J. Kim, and J. Pack, *Dispersive effect of uwb pulse on human head*, Electromagnetic Compatibility, 2007. EMC Zurich 2007. 18th International Zurich Symposium on, 2007, p. 4144.
15. M. Kohandel, S. Sivaloganathan, G. Tenti, and K. Darvish, *Frequency dependence of complex moduli of brain tissue using a fractional zener model*, Physics in Medicine and Biology **50** (2005), no. 12, 2799.
16. J. Li, *A fast time stepping method for evaluating fractional integrals*, Siam J. Sci. Comput. **31** (2010), no. 6, 4696–4714.
17. P. G. Petropoulos, *On the time-domain response of cole-cole dielectrics*, Antennas and Propagation, IEEE Transactions on **53** (2005), no. 11, 3741–3746.
18. I. Podlubny, *Fractional differential equations. an introduction to fractional derivatives, fractional differential equations, some methods of their solution and some of their applications*, Academic Press, San Diego - New York - London, 1999.
19. A. Schmidt and L. Gaul, *Finite element formulation of viscoelastic constitutive equations using fractional time derivatives*, Nonlinear Dynamics **29** (2002), no. 1-4, 37–55 (English).
20. J. C. Strikwerda, *Finite difference schemes and partial differential equations*, Wadsworth Publ. Co., Belmont, CA, USA, 1989.
21. L. Yuan and O.P. Agrawal, *A numerical scheme for dynamic systems containing fractional derivatives*, Journal of Vibration and Acoustics **124** (2002), 321324.